The contribution of hydrogen to the corrosion of 2024 aluminium alloy exposed to thermal and environmental cycling in chloride media

Céline Larignon, Joël Alexis, Eric Andrieu, Grégory Odemer, Christine Blanc

The contribution of hydrogen to the corrosion of 2024 aluminium alloy exposed to thermal and environmental cycling in chloride media

Celine Larignon [a,b], Joel Alexis [b], Eric Andrieu [a], Gregory Odemer [a,*], Christine Blanc [a]

[a] Université de Toulouse, CIRIMAT, UPS/CNRS/INPT, 4 allée Emile Monso, BP 44362, 31030 Toulouse cedex 4, France
[b] Université de Toulouse, INP/ENIT/LGP, 47 avenue d'Azereix, BP 1629, 65016 Tarbes, France

A B S T R A C T

This work is focused on the role of hydrogen in corrosion damage induced by the cyclic exposure of 2024 aluminium alloy to chloride media with air emersion periods at room and/or negative temperatures. Various analysis and microscopic observation techniques were applied at intergranular corrosion defects. A mechanism involving the contribution of hydrogen to the degradation of the alloy mechanical properties is presented. Several consecutive stress states appear during cycling, resulting from volume expansion of the electrolyte trapped in the intergranular defects during emersion phases at −20 °C. These stress states lead to hydrogen diffusion, transport and trapping.

Keywords:
A. Aluminium
B. SIMS
C. Hydrogen absorption
C. Hydrogen embrittlement
C. Intergranular corrosion
C. Stress corrosion

1. Introduction

The aluminium alloys most commonly encountered in airframe construction are the precipitation hardened alloys of the 2xxx series. 2024 aluminium alloy (AA) is the predominant aircraft alloy used in fuselage panels, wing tension members, shear webs and ribs and the structural areas in which stiffness, fatigue resistance and high strength are required. In service-life, these airplane structures can be subjected to complex thermal and environmental cycling, leading to localised corrosion such as pitting corrosion, intergranular corrosion, exfoliation and stress corrosion cracking in chloride-containing environments [1–12].

Based on these consequences, a previous paper [13] focused on the corrosion damage brought about by the cyclic exposure of 2024 aluminium alloy to chloride media. The results showed that, in comparison to continuous immersion, cyclic corrosion testing led to enhanced corrosion damage with a modification of the corrosion defect morphology that depended on the exposure characteristics. For cyclic tests with air exposure periods at room temperature (RT tests), the corrosion defects were significantly longer; for a cyclic test with air exposure periods at low temperatures equal to −20 °C (LT tests), the propagation of corrosion defects was not promoted, but the density of corroded grain boundaries increased. For both types of testing, the corrosion attack extended from the grain boundaries to the subgrain boundaries, and the defects were more branched than those observed after continuous immersion. In the RT tests, the dissolution processes and the morphology of the corrosion damage were consistent with the residual mechanical properties measured. However, the significant decrease in the mechanical properties of AA 2024 after the LT tests cannot be exclusively explained by the degree of corrosion, suggesting that volume degradation of the material could occur close to the corrosion defects. Therefore, hydrogen embrittlement (HE) might be a possible mechanism for the explanation of the singular behaviour of LT samples in comparison to the samples exposed to continuous immersion or RT tests.

The role of the hydrogen produced by corrosion reactions has long been studied in Al-alloys, particularly alloys of the 7xxx series, under stress corrosion cracking (SCC) conditions [14,15]. Kim et al. [16] demonstrated that the propagation of defects under SCC conditions occurred faster if a H_2 recombination poison was introduced into the media. Moreover, recombination of the H_2 molecule is strongly favoured by the acidic local pH at the defect tip, leading to exacerbated hydrogen penetration. The main effect of anodic dissolution is the creation of critical corrosion defects, which localise the plasticity and promote hydrogen adsorption [17].

Haidemenopoulos et al. [18] studied hydrogen adsorption in AA 2024-T351 by means of continuous immersion exfoliation corrosion tests (EXCO tests) and alternating immersion/emersion tests in NaCl (3.5 wt.%) solutions. The immersion tests led to an increase in pit density, followed by exfoliation. The content of desorbed hydrogen was measured using gas-phase chromatography for different immersion times. The increase in desorbed hydrogen during

Corresponding author. Tel.: +33 (0)5 34 32 34 38; fax: +33 (0)5 34 32 34 98.
E-mail address: gregory.odemer@ensiacet.fr (G. Odemer).

http://dx.doi.org/10.1016/j.corsci.2012.12.005

the immersion tests was directly related to the progression of exfoliation corrosion. Moreover, Haidemenopoulos et al. [18] performed heat treatments at 100 °C after corrosion tests and showed that the desorbed hydrogen content followed an asymptotic law that was characteristic of diffusion from the heart of the material to its external surface. For the alternate immersion/emersion tests, no change in the desorbed hydrogen content was noted, likely owing to the insufficient immersion time applied.

Kamoutsi et al. [19] estimated the diffusion coefficient of hydrogen to be approximately 10^{-13} m^2/s for AA 2024-T351 by means of hydrogen content measurements performed at different depths for specimens corroded for 24 h in EXCO media. They showed that hydrogen was produced by corrosion reactions, followed by the trapping of hydrogen in the microstructure. The different hydrogen active traps localised in the microstructure of the AA 2024-T351 were identified using a thermal desorption method. Four traps were distinguished: the first type of trap, called T1, was characterised by the lowest activation temperature (100 °C). The T2, T3 and T4 traps, respectively, were characterised by increasingly elevated activation temperatures (200, 410 and 495 °C). The last three traps were considered to be irreversible because of the existence of critical temperatures, below which no hydrogen evolution takes place; these are in contrast to T1-type traps, which release hydrogen continuously at temperatures close to room temperature. Trapping state T1 has been related to the interstitial lattice sites, and T2 has been associated with the semi-coherent interfaces of the strengthening phases or the incoherent interfaces of dispersoids and the matrix lattice [19,20]. T3 has been attributed to the formation of magnesium hydride, and trapping state T4 starts to release hydrogen at a temperature coinciding with dissolution of the strengthening Al_2CuMg (S) phase. Kamoutsi et al. showed [19] that removal of the corrosion layer led to complete restoration of the yield strength but only partial restoration of ductility. However, removal of the corrosion layer followed by a heat treatment to activate all hydrogen traps led to complete restoration of not only strength but also ductility.

Many studies on pure aluminium and AA 7xxx have focused on the determination of hydrogen diffusion properties, hydrogen trapping and the effect of hydrogen on the mechanical properties [17,20–24]. In these works, hydrogen was generally introduced into the material by immersion tests or cathodic polarisation. The effects of thermal and environmental cycling on airplane structures during service-life have not been considered, and finally, few results are available concerning the effect of hydrogen during the corrosion damage of AA 2xxx under these conditions.

The main aims of the present paper are to study the possible responsibility of hydrogen in the volume degradation of the material, as suspected in a previous work after LT tests, and to propose a mechanism for this process by taking into account the contribution of hydrogen in the corrosion of a 2024 aluminium alloy exposed to thermal and environmental cycling. At first, to decorrelate the effects of hydrogen from those of corrosion, HE susceptibility of the aluminium alloy 2024 T351 is studied on specimens cathodically charged with hydrogen. Then, hydrogen absorption in proximity of the LT corrosion defects is studied in addition to the effect of this absorption on the corrosion damage characteristics. Finally, based on the experimental results, a mechanism is proposed to explain the material damage induced by the LT tests.

2. Experimental

2.1. Material

AA 2024-T351 is an Al–Cu–Mg alloy, provided by Constellium in the form of a 50 mm-thick rolled plate. Its composition by weight is 4.46% Cu, 1.44% Mg, 0.60% Mn and 0.13% Fe [13]. The T351 temper consisted of a solid-solution heat treatment at 495 °C (±5 °C) followed by water quenching, straining and tempering in ambient conditions for 4 days. The final microstructure of the alloy was composed of grains elongated along the rolling direction (L) with average grain dimensions of 700, 300 and 100 μm, respectively, in the longitudinal, long transverse (LT) and short transverse (ST) directions. Analyses and observations of the microstructure showed both intragranular precipitates, such as Al–Cu–Mn–Fe and Al_2CuMg particles, and intergranular precipitates (mainly Al_2CuMg and Al–Cu–Mn). No precipitate-free zone (PFZ) was observed along the grain boundaries in the as-received plate.

2.2. Corrosion tests

As described in a previous paper [13], the electrolyte for the LT corrosion tests consisted of a 1 M NaCl solution prepared with Rectapur chemicals dissolved in distilled water. The cyclic freezing corrosion test consisted of three cycles of 24 h; each cycle was composed of an 8 h immersion in the electrolyte, followed by a 16 h air exposure period at −20 °C. During the air exposure periods, the samples were hung from nylon yarn in a container maintained at −20 °C. The preliminary measurements related to the melting temperature of the chloride-containing solutions showed that, despite the chloride enrichment in the corrosion defects [13], the electrolyte trapped in the intergranular corrosion defects was frozen during the period of exposure to air at −20 °C. Indeed, the melting temperature of the chloride solutions varied from 2 to −16 °C for chloride contents from 0 to 5 M, with 5 M corresponding to the solubility limit for chloride ions in water. The results obtained for the samples exposed to the LT corrosion tests were compared to the data obtained for the RT tests. A given RT test only differed from a given LT test by the temperature during the emersion period; for RT testing, during the air exposure periods, the samples were hung from nylon yarn in a sample glass cabinet, placed in the laboratory and maintained at 22 °C.

2.3. Hydrogen charging

Assuming that the diffusion rate of hydrogen is very low in aluminium alloys, hydrogen was introduced into the material at 150 °C by an electrochemical charging method in a eutectic mixture of molten salts ($NaHSO_4{\cdot}H_2O$ 53.5 wt.% – $KHSO_4$ 46.5 wt.%), as described by Lacombe, Aucouturier and Chêne [25]. The principle governing this electrochemical technique consists of the electrolysis of water in a molten salt bath using a three-electrode system:

$$\text{Anodic reaction}: \quad H_2O + 2SO_4^{2-} \rightarrow 2HSO_4^- + \frac{1}{2}O_2 + 2e^- \tag{1}$$

$$\text{Cathodic reaction}: \quad HSO_4^- + e^- \rightarrow H_{ads} + SO_4^{2-} \tag{2}$$

A constant cathodic potential was applied between the cathode (the specimen) and the anode (the Pt counter electrode) to verify the cathodic reaction on the specimen surface by means of a Voltamaster potentiostat. The surface area of the Pt electrode was ten times the sample surface area. A reference electrode of Ag/Ag^+ in Pyrex, composed of a Ag wire immersed in a small volume of molten salts and separated from the bath by means of a Luggin capillary, was connected to the potentiostat to monitor any change in the cathode potential. A known concentration of Ag^+, *i.e.*, 1 M, was added to the reference compartment as $AgNO_3$. This electrode is the more practical reference electrode in most molten salt media given that silver is

stable at high temperatures and acts as a noble metal in molten salts [26]. Moreover, there are no problems associated with silver oxide formation according to Ellingham's diagram of silver. Chemical analyses performed after the hydrogen charging revealed no silver deposit on the working electrode surface. Compared to traditional reference electrodes whose potential value is stable, this type of reference electrode can present a slight variation in potential of a few dozen millivolts during its use. In this study, the variation in the reference potential during hydrogen charging was equal to ±15 mV. The applied cathodic potential, *i.e.*, −1 V, was chosen in such a way that the value was localised in the middle of the cathodic plateau, as determined by a preliminary potentiokinetic polarisation test. Seeing that the cathodic plateau width was approximately 400 mV, the effects on hydrogen charging of the variation in the reference potential are minimised. It was verified that the current measured in the cell during hydrogen charging was stable for all cathodic charging times. Finally, the hydrogen content measurements were performed systematically after each hydrogen charging, confirming the good reproducibility of the cathodic charging technique for a given charging time.

The hydrogenation power of the molten salt bath is strongly dependent on its ageing and particularly on its water content. To avoid premature water evaporation, a condenser was used to recover the water evaporated from the molten salt bath. An ohmmeter was regularly used to monitor changes in the electrical resistance of the salt, and deionised water was injected into the salt bath to maintain a constant ohmmeter reading, if necessary. All specimens and holders, except the surfaces intended for charging, were coated by thermal resistant silicone sealant to avoid galvanic reaction. After hydrogen charging, the specimens were stored in liquid nitrogen to prevent hydrogen desorption.

Three cathodic charging times were considered, *i.e.*, 7, 24 and 48 h on 0.5 mm-thick samples. The hydrogen contained in the samples was globally quantified using a Horiba EMGA-621W Instrumental Gas Analyser (IGA). The experimental method consists of melting the sample (0.2 g) by heating to approximately 950 °C, followed by analysing the gases based on the thermal conductivity. The detection limit for this technique is approximately 1 ppm in weight.

2.4. Characterisation of the residual mechanical properties of the hydrogenated specimen

Tensile tests were performed on flat tensile specimens (0.5 mm in thickness) on a MTS testing machine equipped with a 5 kN load cell and a constant strain rate of 10^{-3} s^{-1}. The tests were performed on hydrogen-charged specimens with additional tests carried out only on specimens that had been heat treated at 150 °C for 7, 24 and 48 h to identify the effect of heat treatment on the mechanical properties. For each hydrogen charging time, three tensile specimens were tested to check the reproducibility of the results. AA 2024 alloy without hydrogen charging and without heat treatment was considered as the reference.

2.5. Scanning electron microscope (SEM) observations

Observations were carried out with a field emission gun scanning electron microscope (FEG SEM-7000F from JEOL with the incident electron beam maintained between 10 and 15 kV) to carefully examine the corrosion defects and the fracture surfaces of the tensile specimens. For some, elemental spot analysis was performed with an SDD Bruker X flash energy dispersive X-ray spectrometer (EDX).

2.6. Hydrogen mapping by secondary ion mass spectrometry (SIMS) close to corrosion defects generated by thermal and environmental cycling

A SIMS map allowed the lateral distribution of hydrogen around corrosion defects to be quantified. To obtain a SIMS map, a highly focused primary ion beam (Cs^+) was scanned in a raster pattern across the corrosion defect, and the secondary ions were analysed at specific points on a grid pattern over the selected surface area. The image brightness at each point is a function of the relative concentration of the element mapped. The lateral resolution is less than 0.1 μm.

3. Influence of hydrogen on the mechanical properties of the aluminium alloy 2024 T351

3.1. Preliminary calculations

As stated previously, three hydrogen charging times at 150 °C were considered, *i.e.*, 7, 24 and 48 h, based on the preliminary diffusion calculations related to the resolution of Fick's second law.

The obtained hydrogen diffusion profiles are plotted in Fig. 1 using the classical diffusion equation:

$$\frac{C - C_S}{C_0 - C_S} = \mathrm{erf}\left(\frac{x}{2\sqrt{Dt}}\right) \tag{3}$$

where D is the diffusion coefficient of hydrogen (considered to be constant), t is the charging time, x is the hydrogen penetration depth, C_0 is the initial hydrogen concentration ($C_{0(t=0)} = 0$) and C_S is the surface hydrogen concentration ($C_{S(t=0)} = 1$). Two values of the hydrogen diffusion coefficient were considered based on literature results: 1×10^{-7} cm^2/s [27] and 2×10^{-10} cm^2/s [20]. The first value for pure aluminium was found at the temperature of 135 °C, which is close to the temperature of the molten salts used in this work, while the second value holds from 30 to 600 °C for pure polycrystalline aluminium. It is important to note that the materials considered for these diffusion coefficient measurements presented less complex microstructures than AA 2024 for which hydrogen trapping most likely occurs.

The residual hydrogen concentration profiles showed that hydrogen charging durations are sufficient for hydrogenation to occur in the centre of the 0.5 mm-thick samples for $D = 1 \times 10^{-7}$ cm^2/s but not sufficient for 2×10^{-10} cm^2/s. It should be kept in mind that the calculations are based on approximations and do not take hydrogen trapping into account. Hence, it is very likely that effective hydrogen charging can differ from the theoretical results.

3.2. Hydrogen effects on the mechanical properties of AA 2024-T351

The results of the tensile tests are presented in Fig. 2. The tensile curves obtained for the hydrogen charged samples are compared to those obtained for the samples heat-treated at 150 °C for the same duration as that of the corresponding hydrogen charging time, allowing for the possible results of microstructural ageing in the alloy during cathodic charging at 150 °C to be considered.

The residual mechanical properties are summarised in Table 1. For clarity, the tensile curves corresponding to the non-heat treated and non-hydrogen charged samples (the reference samples) are not plotted in Fig. 2, but the mechanical properties of these reference samples are given in Table 1.

The tensile results show that the longest heat treatment at 150 °C led to modifications in the mechanical properties of the AA 2024 alloy, as expected from the abundant literature data. A comparison between the tensile curves obtained for the hydro-

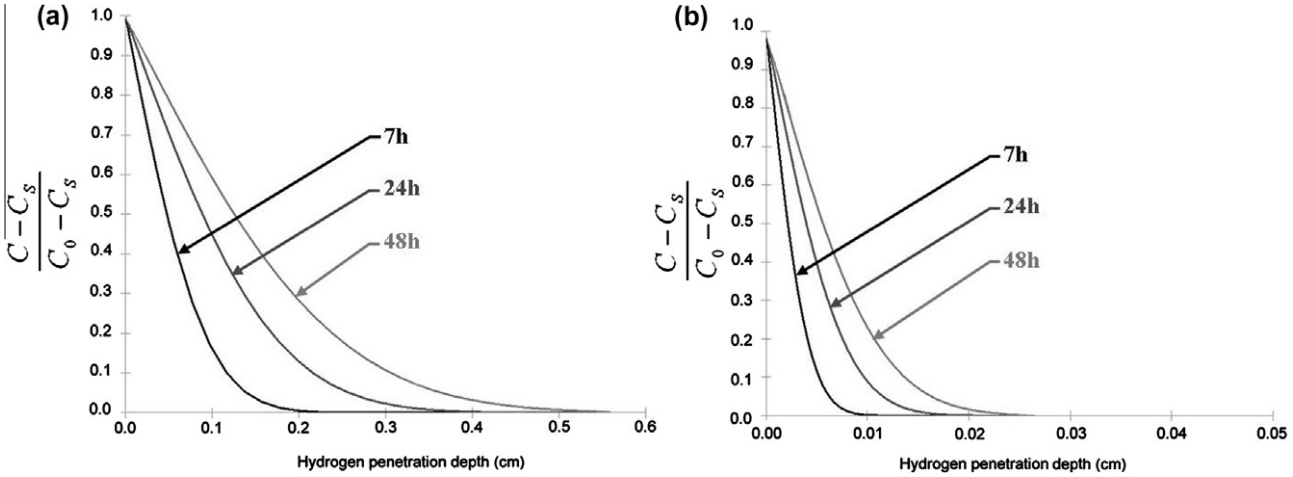

Fig. 1. The residual hydrogen concentration profiles after loading for 7, 24 and 48 h at 150 °C with (a) $D = 1 \times 10^{-7}$ cm^2/s [26] and (b) $D = 2 \times 10^{-10}$ cm^2/s [20].

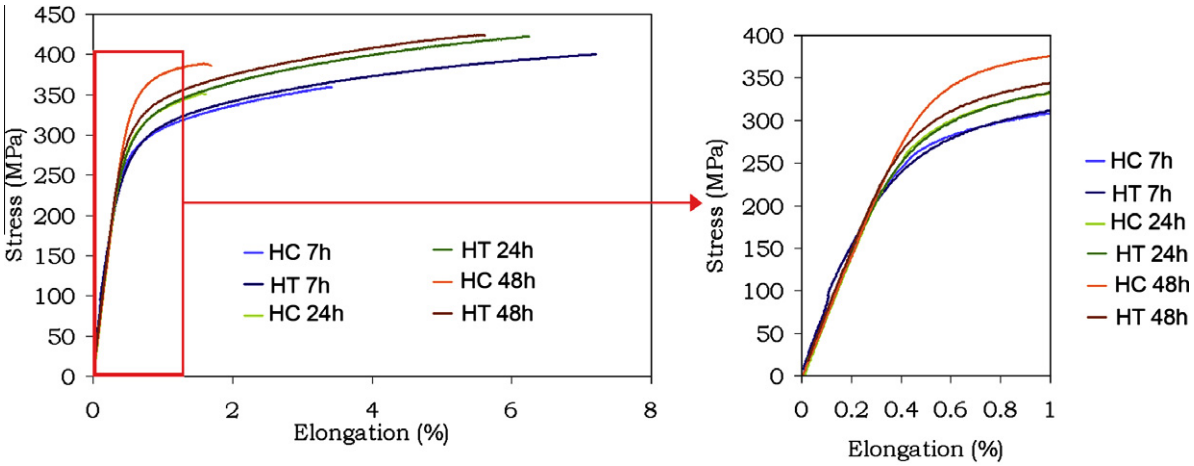

Fig. 2. The tensile curves of the hydrogen-charged (HC) and heat-treated (HT) AA 2024 samples (10^{-3} s^{-1}).

Table 1
The residual mechanical properties of the hydrogen charged and heat-treated AA 2024 samples.

Sample treatments			
Hydrogenation conditions and/or heat treatment conditions	Ultimate tensile strength (MPa)	Yield strength (MPa)	Elongation to failure (%)
H-free			
No heat treatment	430	290	7.2
Heat-treated 7 h/150 °C	400	288	6.9
Heat-treated 24 h/150 °C	425	316	7
Heat-treated 48 h/150 °C	418	331	5.7
Charged 7 h	359	289	3.4
Charged 24 h	355	316	1.7
Charged 48 h	392	362	1.7

gen-charged samples and those for the samples that were only heat-treated provides data related to the role of hydrogen with respect to the mechanical properties of the obtained alloy. Hydrogen was found to have no effect on the stiffness of the material. However, for all hydrogen-charged samples, a strong decrease in the elongation to failure was observed with respect to the only heat-treated samples. The elongation to failure was found to decrease from 3.4% to 1.7% when the hydrogen charging duration was increased from 7 to 24 h and then stabilised for the charging times between 24 and 48 h. A modification in yield strength due to hydrogen was only significant for a charging duration of 48 h; for shorter charging durations, the yield strength was the same for the hydrogen-charged samples and the corresponding heat-treated specimens.

It can be assumed that hydrogen charging induced the formation of a hydrogen-enriched layer near the external surface of the sample. As a result, the hydrogenated specimen can be considered to be a healthy core of material that is similar to a heat-treated AA 2024-T351 but with an external layer affected by hydrogen. Assuming that this external layer was thick enough in comparison

to the bearing surface, an increase in the global yield strength could be obtained for small strains. This occurred for a charging time of 48 h but not for either of the two shorter charging times. With increased strain, this layer could become a preferential zone for crack initiation and/or localised plasticity and, finally, could lead to premature tensile rupture and thus to lower elongation to failure values. This hypothesis is discussed in more detail in the following part of the manuscript, which is focused on the effect of hydrogen on fracture modes. The decrease in the elongation to failure due to hydrogen is commonly observed in the literature [28,29]. For small absorbed hydrogen contents, this effect is related to a solution strengthening mechanism. However, in this work, the significant decrease in the observed elongation to failure suggests that another mechanism could occur in parallel due to the high hydrogen content introduced by cathodic charging (5 ppm by weight for the reference samples, 16 ppm by weight for a 7 h-hydrogen charging, 22 ppm by weight for a 24 h-hydrogen charging and 27 ppm by weight for a 48 h-hydrogen charging). This additional mechanism could be related to hydrogen trapping; as stated previously, this hypothesis is discussed later in the paper based on the corresponding SEM observations.

The increase in the yield strength of a hydrogenated aluminium alloy is not consistent with the results found in other works concerning AA in the 5xxx and 7xxx series [28–30], where an antagonistic effect was found. Nevertheless, for these works, the applied strain rates were very low in comparison to the strain rate of the present work ($10^{-3}\ s^{-1}$). It is widely recognised that strain rate is a fundamental parameter in the HE susceptibility of a metal alloy. Indeed, low strain rates ($\approx 10^{-5}\ s^{-1}$) favour interactions between hydrogen and dislocations, and thus, low strain rates also favour the localisation of plasticity, inducing a strong decrease in the mechanical properties. Hence, it is difficult to directly compare the results obtained in the data presented here to those reported elsewhere. Nevertheless, other studies on pure aluminium have found a similar effect [31] to that reported in this study, explaining the observation with the high density of dislocations in the hydrogen-enriched zones.

3.3. The effects of hydrogen on the fracture surfaces of AA 2024-T351

The fracture surfaces of the hydrogen charged tensile specimens were observed with SEM. Regardless of the hydrogen charging duration, the same type of fracture mode was observed for each sample. Fig. 3a presents a characteristic SEM observation of the global fracture surface corresponding to a 48 h hydrogen charging. Two typical zones can be seen: at the centre of the sample, the fracture mode was found to be ductile with typical dimples, while a smooth fracture surface was found at the periphery with the magnification used here. The hydrogen charging duration directly influenced the depth of this external layer, which increased as the charging duration increased, related to the quantity of hydrogen introduced during charging. A more detailed observation (Fig. 3b) of this external layer showed that this zone was not at all smooth but presented smaller dimples in comparison with those observed in the centre of the tensile specimen. Moreover, the size of the dimples increased with increasing distance from the external surface of the sample. The evolution of the dimple size could be related to the hydrogen concentration profile in the material and strongly suggests hydrogen embrittlement of the strengthening precipitates and/or interface matrix/precipitates, as shown by Kamoutsi et al. [19].

Assuming that the hydrogen trapped at the matrix/precipitate interfaces can partially relax the coherency stresses but also can decrease the local cohesion energy at the matrix/precipitate interfaces, nucleation of cavities and growth is then possible. In Fig. 4, a SEM micrograph of the dimples (Fig. 4a) is compared to SEM (Fig. 4b) and TEM (Fig. 4c) micrographs of the intragranular precipitates observed in the AA 2024 T351. Two scales of intragranular precipitates were observed, *i.e.*, coarse (3–15 μm) and fine (100–600 nm) particles. It is worth noting that the scale of the inclusions

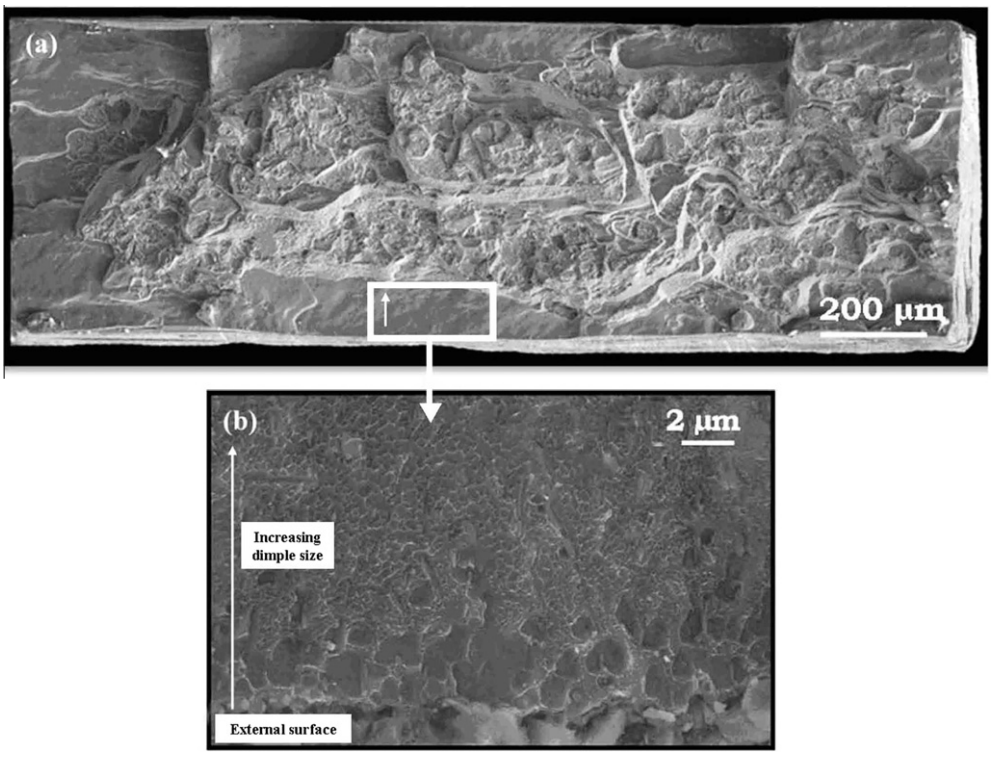

Fig. 3. SEM observations of the fracture surface for a 48 h-hydrogenated sample (strain rate: $10^{-3}\ s^{-1}$): (a) the global view and (b) focused on the external layer.

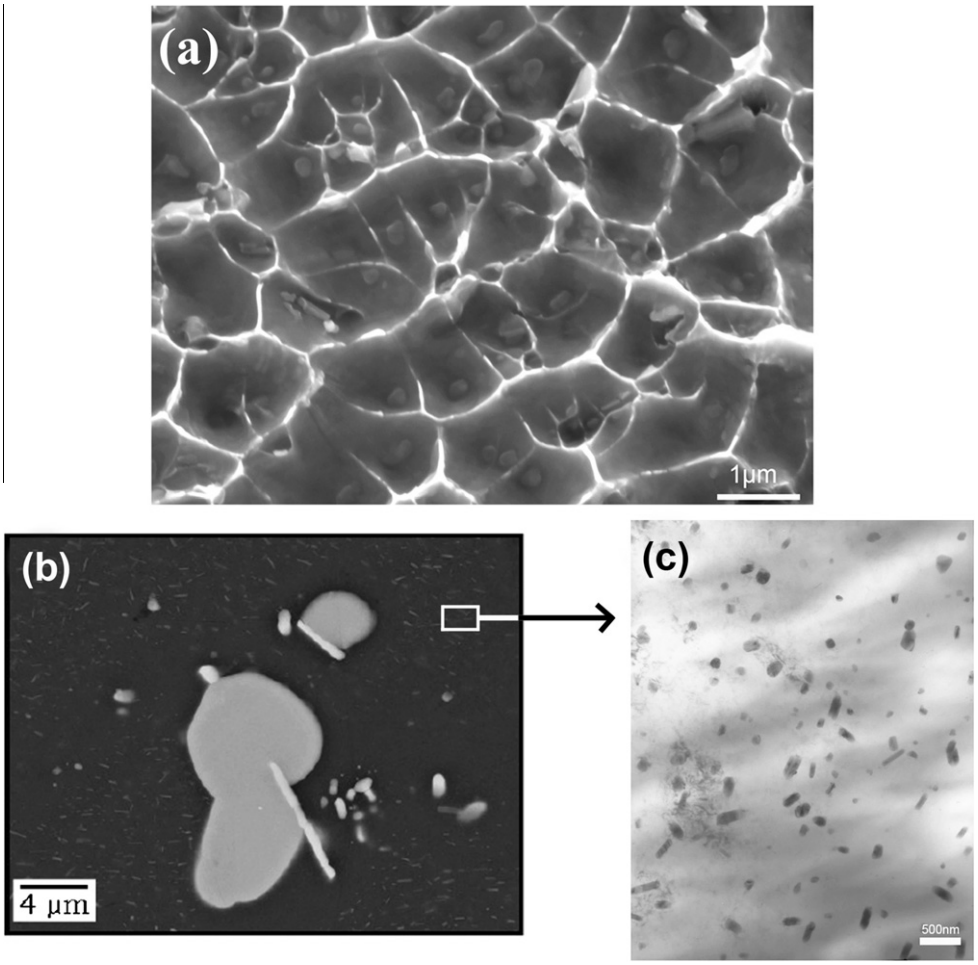

Fig. 4. (a) SEM observation of dimples in the hydrogen-affected external layer for a hydrogen loading of 48 h, (b) SEM observation of the intragranular coarse precipitates and (c) TEM observation of the intragranular fine precipitates of AA2024-T351.

Table 2
The apparent hydrogen diffusion coefficients of AA2024-T351 calculated for different charging times at 150 °C.

Hydrogen charging time (h)	Apparent hydrogen diffusion coefficient at 150 °C (cm^2/s)
7	4.4×10^{-10}
24	1.6×10^{-9}
48	1.4×10^{-6}

in the dimples is significantly different from the size of the coarse particles but is also very close to the size of the fine precipitates. It is then reasonable to describe the fracture process in this area as a classical ductile fracture mechanism with cavity nucleation, followed by plastic growth and finally coalescence. Because the precipitates are close to one another, the fracture roughness is so small that it looks smooth when observed at lower magnifications. This observation is consistent with those reported in other works concerning the HE of steels [32] and 7xxx aluminium alloys [28]. Hydrogen trapping seems to favour the nucleation of cavities, leading to lower values of elongation to failure as characterised by tensile tests.

The apparent hydrogen diffusion coefficients were determined from the depth of the hydrogen-enriched external layer and are summarised in Table 2. The values varied between the hydrogen charging times. Diffusion is a thermally activated process, which implies that the apparent hydrogen diffusion coefficients should be constant for a given temperature regardless of the charging time. In this work, the apparent hydrogen diffusion coefficients were found to depend on the hydrogen charging time, suggesting that hydrogen mobility is not governed only by a diffusion mechanism. These experimental tests show the efficiency of other mechanisms, such as hydrogen trapping and/or the accelerated diffusion of hydrogen along grain boundaries.

Following the demonstration that AA 2024-T351 is susceptible to hydrogen embrittlement (HE), it was necessary to study the production and the absorption of hydrogen during corrosion reactions and their effects on corrosion defect morphology.

4. Hydrogen absorption in proximity of corrosion defects after continuous immersion and thermal and environmental cycling in chloride-containing solutions

In a previous report [13], hydrogen content measurements revealed hydrogen enrichment after corrosion tests following either 24 or 72 h of continuous immersions; similar results were found after thermal and environmental cycling. It was determined that the results were related to acidification at the intergranular corrosion front, followed by hydrogen absorption and diffusion in the vicinity of the corrosion defect. To confirm hydrogen penetration, SIMS analyses were performed around the LT corrosion defects.

4.1. Local SIMS analysis of hydrogen penetration in proximity to the corrosion defects

In reference to measurements of the hydrogen content [13], it appeared that hydrogen penetration was more pronounced in the LT tests. This was assumed to be due to the presence of an additional mechanical effect, which improved the trapping and diffusion of hydrogen into the material; this effect is discussed later in the manuscript. Therefore, SIMS mapping was focused on the LT corrosion conditions. To distinguish between a hydrogen signal coming from corrosion products (hydroxides) and the atomic hydrogen signal, signals of oxygen and hydrogen were followed in parallel. The SIMS maps are presented in Fig. 5. Fig. 5a and b correspond to the hydrogen and oxygen maps, respectively, obtained close to an intergranular corrosion defect that developed during LT testing. Fig. 5c and d correspond to the hydrogen and oxygen maps, respectively, obtained close to a corrosion defect developed during LT testing in which the grain and subgrain boundaries are corroded.

Maps (a) and (b) show that the hydrogen and oxygen signals are correlated; this suggests that the hydrogen signal due to atomic hydrogen penetration cannot be decorrelated from the hydrogen signal coming from the corrosion products. Therefore, it is impossible to develop conclusions from these results concerning the penetration of atomic hydrogen into the material. However, maps (c) and (d), performed close to a point of corrosion affecting both grain and subgrain boundaries, clearly show a high hydrogen signal in the subgrain boundaries zone, which is associated with a weak oxygen signal. This strongly suggests hydrogen enrichment in these zones. Therefore, SIMS analyses confirm the hydrogen penetration and diffusion through material. Indeed, hydrogen seems to be present in the material under two states, *i.e.*, as a constitutive element of the corrosion products and under atomic form in solid solution, particularly in the subgrain boundaries, which can be considered to be diffusion short-circuits. The presence of hydrogen in the subgrain boundaries could modify their susceptibility to localised corrosion. This could be an explanation for the morphology defects that occurred during the LT tests: the subgrain boundaries were found to be corroded after the LT tests, which was not observed after continuous immersion tests. Additionally, the effect of the chloride ion concentration cannot fully explain the subgrain attack [13].

Following the demonstration that hydrogen is absorbed during corrosion reactions and penetrates into the material surrounding the corrosion defects, the effect of hydrogen on the fracture modes was studied.

4.2. SEM observations of the corrosion defects that occurred during thermal and environmental cycling

The fracture surfaces of the tensile specimens were pre-corroded during the cyclic immersion tests (the LT tests), followed

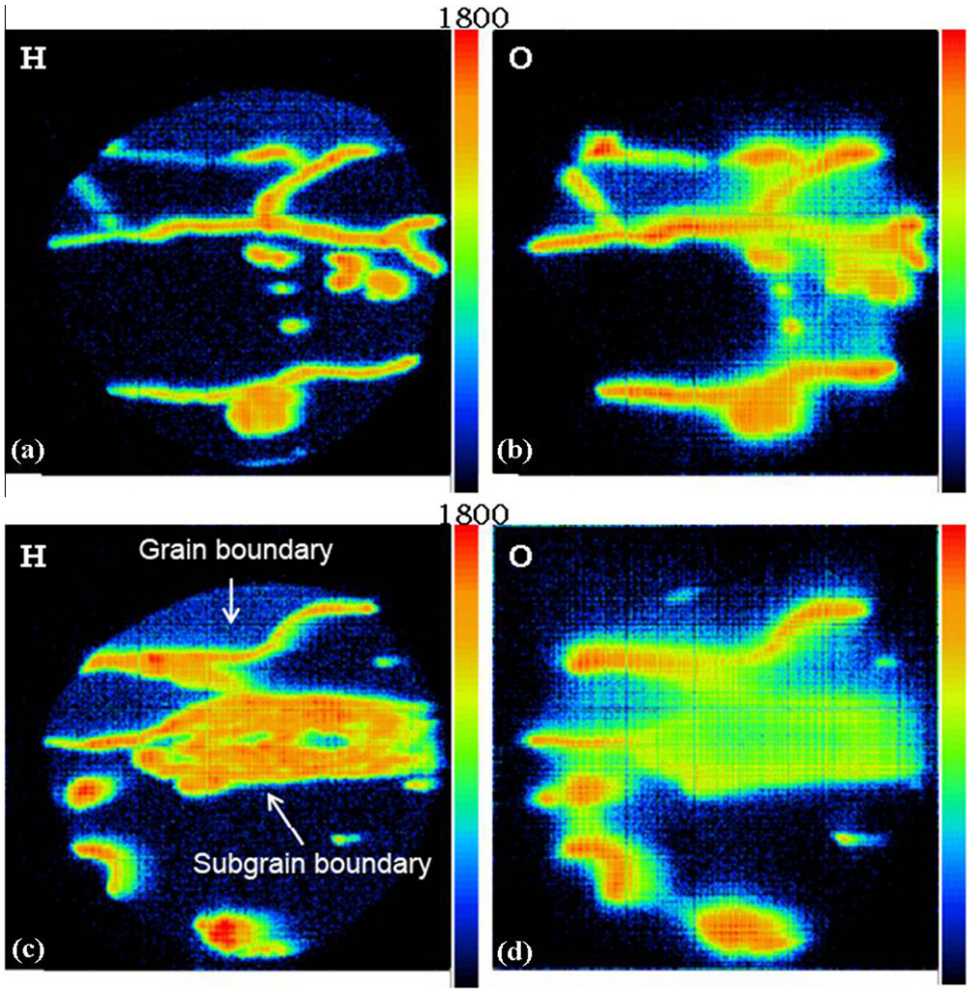

Fig. 5. (a) and (b) SIMS analyses around an intergranular corrosion defect generated by LT testing: (a) hydrogen and (b) oxygen maps; (c) and (d) SIMS analyses around a corrosion defect generated by LT testing; this corrosion defect propagated in the grain boundaries and in the subgrain boundaries: (c) hydrogen and (d) oxygen maps.

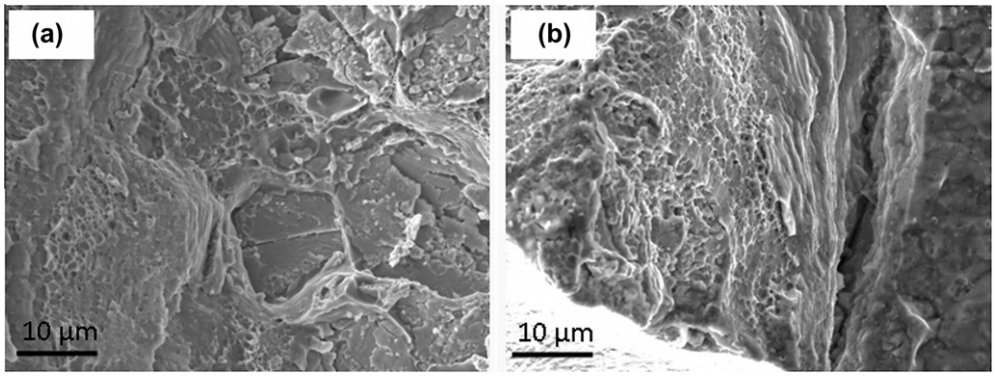

Fig. 6. SEM observations of the fracture surface (strain rate: 10^{-3} s^{-1}) of the AA2024 T351 sample pre-corroded under (a) RT conditions and (b) LT conditions.

by SEM observation. During SEM inspection, attention was paid to the area adjacent to the corrosion defects (Fig. 6a and b). A fracture surface obtained after RT testing is shown for comparison (Fig. 6a).

Numerous dimples can be observed close to the intergranular defects that formed during the cyclic corrosion tests (RT and LT). Their sizes vary from approximately 2–10 µm for the RT testing conditions to submicron sizes for the LT tests. According to the results previously presented in this study with respect to the specific fracture behaviour of cathodically hydrogen-charged samples, the presence of microdimples for the LT samples suggested local hydrogen enrichment. During the periods of immersion in the chloride solution, the corrosion reactions led to hydrogen production. Hydrogen diffused into the material and was trapped at the matrix/strengthening phase interfaces, leading to embrittlement of the interface matrix/precipitates responsible for cavity nucleation during tensile testing.

It was interesting to compare the fracture surfaces obtained for the LT-pre-corroded tensile specimen with the SEM micrographs obtained from specific zones of the samples corroded during LT testing. The latter samples are cubic specimens previously exposed to a LT test. The specimens were then cut perpendicularly to the surface exposed to the electrolyte and mechanically polished on the cross section to observe the propagation of corrosion. Fig. 7 presents a LT intergranular corrosion defect from which a grain has been removed, likely due to the mechanical polishing step. Typically sized dimples were observed in the defects related to the presence of intermetallic particles and inclusions in the microstructure of AA 2024-T351 (Fig. 7a). However, a magnified view of this area (Fig. 7b) clearly shows a second dimple size scale (<1 µm). Investigation of the tearing zone (Fig. 7c and d) reveals the presence of additional small-size dimples. Therefore, several similarities were observed between the fracture surfaces obtained on the cathodically hydrogen-enriched tensile specimens and those of the LT pre-corroded tensile specimens and the LT corroded cubic samples. The results strongly suggest that mechanisms linked to a hydrogen effect could be involved in the LT test.

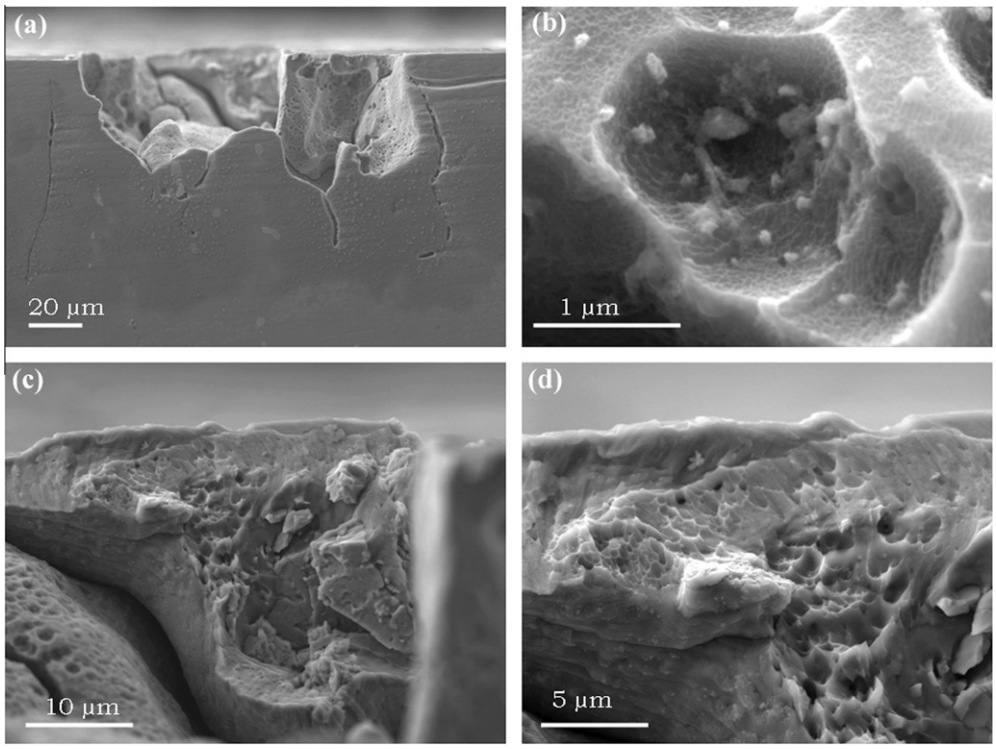

Fig. 7. SEM observations of a corrosion defect grown during LT testing: (a) a global view, (b) a magnified image of the dimples, (c) the tearing zone and (d) a magnified image of the tearing zone.

Based on the experimental results presented in this work concerning the effect of hydrogen penetration during corrosion reactions and by taking into account the results given in a previous paper [13] on corrosion damage induced by cyclic exposure, a mechanism explaining the contribution of hydrogen in the corrosion damage of a AA 2024-T351 aluminium alloy exposed to the LT tests is proposed.

5. On the role of hydrogen in the mechanisms of corrosion of AA 2024-T351 exposed to thermal and environmental cycling

A previous work [13] dealing with the evaluation of mechanical stresses inside corrosion defects formed during the LT tests concluded that the electrolyte and/or the corrosion products trapped inside the corrosion defects generate strong tensile stresses during periods of emersion at −20 °C due to volume expansion as a result of freezing. Moreover, the hydrogen content was significantly higher in the LT specimens than in the RT specimens and in samples exposed to continuous immersion tests. The quantity of hydrogen Q_H introduced by corrosion reactions in the alloy can be considered as the product of a flow ϕ, an exposure time t to hydrogen and an exchange surface area S. An increase in the hydrogen content implies that at least one of the three parameters has increased in value. The exposure time cannot be increased in the LT tests due to stopping of the electrochemical reactions during the emersion periods at −20 °C; therefore, for LT tests, the entire exposure time to hydrogen was only 24 h, which corresponds to the duration of the immersion period. The flow ϕ can be expressed by the following expression, which includes a diffusion term and a transport contribution (T):

$$\phi = -D\left(\frac{dC_H}{dx}\right) + T \quad (4)$$

After considering that occlusion of the intergranular defects by the corrosion products and acidification processes is the same for both the RT and LT tests, then no variation in the hydrogen concentration gradient C_H can be considered. The diffusion coefficient D is essentially affected by dislocations. However, dislocations are hydrogen traps, which tend to decrease the quantity of hydrogen introduced. Therefore, this parameter cannot explain the higher hydrogen content that occurred as a result of the LT tests. With respect to the contribution of the transport T, the existence of mobile dislocations is a requirement. However, hydrogen is produced during immersion phases when the material is not subjected to stresses, which could modify the dislocation mobility. Therefore, the exchange surface area S is the only parameter able to increase the quantity of hydrogen in LT tests. An increase in the value of S is consistent with local rupture of the oxide film along the walls of the corrosion defects due to the expansion of frozen electrolyte trapped within the defects.

Based on this, a mechanism was suggested. During the first immersion period of the cycle (the first 8 h of immersion in the chloride solution), electrochemical processes led to the formation of an occluded zone at the tip of the intergranular defects, characterised by a chloride-rich electrolyte and H^+ reduction as the major cathodic reaction. Aluminium alloy can be schematically described as a material composed of a base metal core without damage (WD) and a surface zone damaged (D) altered by corrosion phenomena (Fig. 8a). At the end of the first immersion period, the sample is placed in a chamber at −20 °C. At this temperature, electrochemical processes are considered to be rapidly stopped. As long as the temperature is above the melting temperature (T_m) of the electrolyte trapped inside the corrosion defects, no stresses occur in the material. If the temperature falls below T_m, the solution freezes and several phenomena occur. At first, due to expansion of the frozen electrolyte, local ruptures in the oxide film appear. On the material surface, the zones of oxide film rupture become preferential zones for the initiation of corrosion defects during the next immersion period in corrosive media. The same assumption can be proposed for local ruptures in the oxide film occurring on the walls of the corrosion defects. This explains the fact that, for LT tests, a high density of corrosion defects was observed at the end of the LT cyclic tests. Moreover, in the intergranular defects, local ruptures in the oxide film on the walls of the corrosion defects become preferential zones for hydrogen absorption because hydrogen was previously produced during the immersion period. Therefore, the exposure to negative temperature leads to an increase in the exchange surface between the hydrogen-rich medium and the material. At the macroscopic scale, expansion of the frozen electrolyte provides an apparent negative expansion coefficient to the damaged zone, while the zone without damage has a tendency to contract. These strain incompatibilities lead to compressive stresses in the damaged zone and tension stresses in the zone without damage (Fig. 8c). The amplitude of these stresses depends on the proportion of the damaged zone in comparison to the zone without damage and could lead to plasticisation of the sample core, if the corroded zones are sufficiently deep and/or the material specimen is sufficiently thin. At a local scale, the stresses are exacerbated at the defect tips due to the notch effect (Fig. 8b). At the defect tip, the stresses in the plastic zone are higher than the yield strength, which leads to plasticisation of the material. The plasticisation sets in motion the dislocations present in the material and contributes to the generation of new dislocations. Mobile dislocations can transport hydrogen, and the new dislocations increase the density of hydrogen traps, which will be active during the next immersion step. Moreover, mechanical propagation of the corrosion defects due to these local stresses is also possible, depending

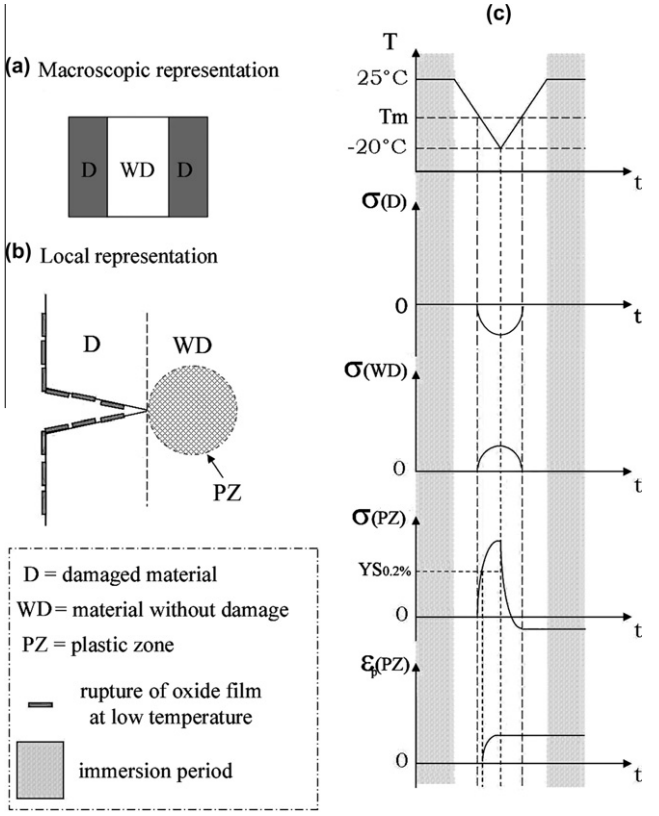

Fig. 8. The damage mechanisms during LT tests: (a) a macroscopic representation of the damaged material, (b) a local representation of an intergranular corrosion defect and (c) a schematic evolution of the local and global stresses and strains during LT testing.

on the stress level and the grain boundary cohesion, which might have been weakened by hydrogen and/or by selective anodic dissolution. The propagation of the corrosion defects, assisted by stresses, leads to a shift in the hydrogen source toward the centre of the material during the next immersion period; this mechanism would be consistent with the hypothesis of volume degradation, as suggested by Pantelakis et al. [33] When the sample is re-immersed in the chloride solution (the second and third immersion periods), the stresses disappear with the elevated temperature, which could close the corrosion defects. However, because the material at the tip of the defect has been plasticised, a plastic strain remains in the location (ε_p(PZ)). This residual strain induces compressive stress in the plasticised zone. Some works have shown that compressive stresses equal to 50% of the yield strength tend to decrease the propagation of intergranular defects [34,35]. At the tip of the corrosion defects, the extent of the plasticised zone is low, and the compressive stresses are most likely lower than 50% of the yield strength, which could explain the continued propagation of the corrosion defects. However, the existence of the compressive stress could favour other propagation paths, such as grain and subgrain boundaries not affected by the plastic zone or close to rupture, in the oxide film. Therefore, this mechanism could explain the increased branching of intergranular defects observed after the LT tests.

Finally, hydrogen diffusion is also possible during emersion phases at 25 °C in parallel to hydrogen transport processes occurring during emersion periods at negative temperatures.

For RT tests and continuous immersions tests, the low hydrogen content measured suggests that no hydrogen transport process is active. The stresses induced by the hydrated corrosion products present inside the corrosion defects must be highly limited, allowing only the hydrogen diffusion processes to occur. Moreover, the oxide film must be a strong barrier to the penetration of hydrogen in the absence of volume expansion in the frozen electrolyte and the stresses between the oxide layer and the underlying material. This conclusion can be supported by the works of Hardwick et al., who were unable to show HE for 2124 aluminium alloy without applied stresses [36].

6. Conclusions

The contribution of hydrogen to the corrosion of AA 2024-T351 exposed to thermal and environmental cycling in chloride media was studied. This work confirmed the production and penetration of hydrogen during corrosion reactions. The fracture surfaces and residual mechanical properties of the cathodically hydrogen-enriched samples showed numerous similarities to those of samples corroded during the LT tests. For samples exposed to LT testing, hydrogen trapping at the matrix/strengthening phase interface was observed on the fracture surfaces and around the corrosion defects. Moreover, SIMS mapping highlighted the hydrogen enrichment along the subgrain boundaries. Finally, a mechanism was proposed to describe the results obtained for the LT tests. The mechanism is based on the interaction between the electrochemical and mechanical processes related to the immersion/emersion phases. The existence of mechanical stresses induced by the expansion of frozen electrolyte trapped inside the corrosion defects seems necessary to observe a significant hydrogen contribution to the corrosion mechanisms occurring in AA 2024-T351.

Acknowledgements

This work was financially supported by the Conseil Régional de la Région Midi-Pyrénées and the Ministère de l'Industrie in the framework of the Diagnostat project. The authors thank S. Rolet (EADS IW) and S. Van-Der-Veen (Airbus) for their help.

References

[1] C. Blanc, G. Mankowski, Corros. Sci. 40 (1998) 411–429.
[2] Z. Szklarska-Smialowska, Corros. Sci. 41 (1999) 1743–1767.
[3] N.D. Alexopoulos, Mater. Sci. Eng., A 520 (2009) 40–48.
[4] W. Zhang, G.S. Frankel, Electrochim. Acta 48 (2003) 1193–1210.
[5] J.R. Galvele, Corros. Sci. 47 (2005) 3053–3067.
[6] V. Guillaumin, G. Mankowski, Corros. Sci. 41 (1999) 421–438.
[7] J.R. Galvele, S.M. De Micheli, Corros. Sci. 10 (1970) 795–807.
[8] C. Augustin, E. Andrieu, C. Blanc, G. Mankowski, J. Delfosse, J. Electrochem. Soc. 154 (2007) 637–644.
[9] W. Zhang, G.S. Frankel, J. Electrochem. Soc. 149 (2002) 510–519.
[10] M.R. Bayoumi, Eng. Fract. Mech. 54 (1996) 879–889.
[11] X. Liu, G.S. Frankel, B. Zoofan, S.I. Rokhlin, J. Electrochem. Soc. 153 (2006) 42–51.
[12] K. Urushino, K. Sugimoto, Corros. Sci. 19 (1978) 225–236.
[13] C. Larignon, J. Alexis, E. Andrieu, C. Blanc, G. Odemer, J.-C. Salabura, J. Electrochem. Soc. 158 (2011) 1–12.
[14] T.D. Burleigh, Corrosion J. 47 (1991) 89–98.
[15] W. Gruhl, Aluminum 54 (1978) 323–325.
[16] H.P. Kim, S.I. Pyun, R.H. Song, Br. Corros. J. 23 (1988) 254–258.
[17] D. Najjar, T. Magnin, T.J. Warner, Mater. Sci. Eng., A 238 (1997) 293–302.
[18] G.N. Haidemenopoulos, N. Hassiotis, G. Papapolymerou, V. Bontozoglou, Corrosion 54 (1998) 73–78.
[19] H. Kamoutsi, G.N. Haidemenopoulos, V. Bontozoglou, S. Pantelakis, Corros. Sci. 48 (2006) 1209–1224.
[20] G.A. Young, J.R. Scully, Acta Mater. 46 (1998) 6337–6349.
[21] T. Ishikawa, R.G. McLellan, Acta Metall. Mater. 34 (1986) 1091–1095.
[22] S.W. Smith, J.R. Scully, Metall. Mater. Trans. A 31 (2000) 179–193.
[23] C. Wolverton, V. Ozolins, M. Asta, Phys. Rev. B 69 (144109) (2004) 1–16.
[24] H.J. Schlüter, H. Züchner, R. Braun, H. Buhl, Z. Phys. Chem. 181 (1993) 103–109.
[25] P. Lacombe, M. Aucouturier, J. Chêne, Hydrogen trapping and hydrogen embrittlement, in: R. Gibala, R.F. Hehemann (Eds.), Hydrogen Embrittlement and Stress Corrosion Cracking, ASM International, 2002, pp. 79–80.
[26] J. O'M Bockris, G.J. Hills, D. Inman, L. Young, J. Phys. E: Sci. Instrum. 33 (1956) 438–439.
[27] H. Saitoh, Y. Lijima, H. Takana, Acta Metall. Mater. 42 (1994) 2493–2498.
[28] N. Takano, Mater. Sci. Eng., A 483 (2008) 336–339.
[29] A.S. El-Amoush, J. Alloys Compd. 438 (2007) 222–231.
[30] M.B. Kannan, V.S. Raja, J. Mater. Sci. 41 (2006) 5495–5499.
[31] J.W. Watson, Y.Z. Shen, M. Meshii, Metall. Trans. A 19 (1988) 2299–2304.
[32] C.D. Beachem, Metall. Mater. Trans. B 3 (1972) 441–455.
[33] S.G. Pantelakis, P.G. Daglaras, C.A. Apostolopoulos, Theor. Appl. Fract. Mech. 33 (2000) 117–134.
[34] C. Augustin, Ph.D. thesis, Prévisions des cinétiques de propagation de défauts de corrosion affectant les structures en alliages d'aluminium 2024, Institut National Polytechnique de Toulouse, France (2008).
[35] X. Liu, G.S. Frankel, Corros. Sci. 48 (2006) 3309–3329.
[36] D.A. Hardwick, M. Taheri, A.W. Thompson, I.M. Bernstein, Metall. Trans. A 13 (1982) 235–239.